JOC The Journal of Organic Chemistry
Cite This: J. Org. Chem. 2019, 84, 14670−14678
Article
pubs.acs.org/joc

Maltol- and Allomaltol-Derived Oxidopyrylium Ylides: Methyl Substitution Pattern Kinetically Influences [5 + 3] Dimerization versus [5 + 2] Cycloaddition Reactions

Lauren P. Bejcek,[†,‡] Aswin K. Garimallaprabhakaran,[†] Duygu M. Suyabatmaz,[†] Alexander Greer,[†,‡] William H. Hersh,[‡,∥] Edyta M. Greer,*[,§] and Ryan P. Murelli*[,†,‡]

[†]Department of Chemistry, Brooklyn College, The City University of New York, Brooklyn, New York 11210, United States
[‡]PhD Program in Chemistry, The Graduate Center of the City University of New York, New York, New York 10016, United States
[§]Department of Natural Sciences, Baruch College, City University of New York, New York, New York 10010, United States
[∥]Department of Chemistry and Biochemistry, Queens College, City University of New York, Queens, New York 11367, United States

Supporting Information

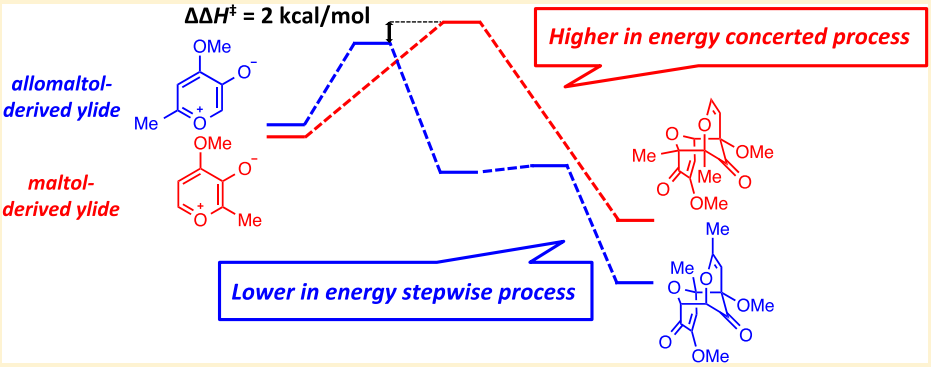

ABSTRACT: Oxidopyrylium ylides are useful intermediates in synthetic organic chemistry because of their capability of forming structurally complex cycloadducts. They can also self-dimerize via [5 + 3] cycloaddition, which is an oft-reported side reaction that can negatively impact [5 + 2] cycloadduct yields and efficiency. In select instances, these dimers can be synthesized and used as the source of oxidopyrylium ylide, although the generality of this process remains unclear. Thus, how the substitution pattern governs both dimerization and cycloaddition reactions is of fundamental interest to probe factors to regulate them. The following manuscript details our findings that maltol-derived oxidopyrylium ylides (i.e., with ortho methyl substitution relative to oxide) can be trapped prior to dimerization more efficiently than the regioisomeric allomaltol-derived ylide (i.e., with a para methyl substitution relative to oxide). Density functional theory studies provide evidence in support of a sterically (kinetically) controlled mechanism, whereby gauche interactions between appendages of the approaching maltol-derived ylides are privileged by higher barriers for dimerization and thus are readily intercepted by dipolarophiles via [5 + 2] cycloadditions.

INTRODUCTION

[5 + 2] Cycloaddition reactions between oxidopyrylium ylide intermediates and dipolarophiles generate bicyclic compounds of synthetic use (i.e., **1** → **3**, Scheme 1), including highly functionalized natural products.[1] Oxidopyrylium ylide intermediates also have the capacity to dimerize through a [5 + 3] cycloaddition in their neutral form (i.e., **1** → **4**, Scheme 1),[2,3] which is an important process that is in need of more study. A mechanistic understanding of factors that influence oxidopyrylium ylide dimerization is potentially of high value due to the difficulty in controlling the otherwise reactive state of the neutral form.

Our lab has previously focused on intermolecular [5 + 2] cycloaddition reactions with oxidopyrylium ylides generated via deprotonation of kojic acid (**5**)-derived methyl triflate salts (Scheme 2), first described by Wender.[3] During the course of these studies, it was revealed that dimer **8** generally forms instantaneously upon the treatment of base, even in the presence of reactive dipolarophiles, but over time, can convert into cycloadducts (i.e., **10**).[4] While it has been proposed that the conversion of the oxidopyrylium dimer to cycloaddition products proceeds by way of cycloreversion back to oxidopyrylium ylides (i.e., $7^{(-)}$),[5] a confounding problem in the validation of this mechanistic hypothesis has been the inability to directly detect the ylides due to their highly reactive

Received: August 20, 2019
Published: October 11, 2019

Downloaded via BROOKLYN COLG on May 29, 2020 at 18:08:35 (UTC).
See https://pubs.acs.org/sharingguidelines for options on how to legitimately share published articles.

© 2019 American Chemical Society

DOI: 10.1021/acs.joc.9b02137
J. Org. Chem. 2019, 84, 14670−14678

Scheme 1. General Representation of Oxidopyrylium [5 + 2] Cycloaddition Chemistry, and the Known Dimerization Product of Oxidopyrylium Ylide 1

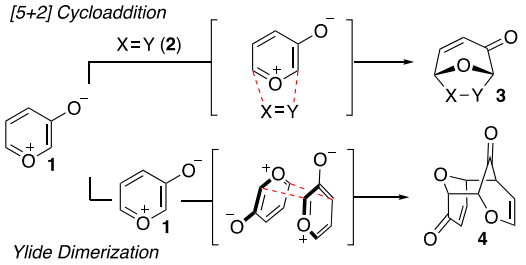

Scheme 2. Kojic Acid-Derived Oxidopyrylium Salt 7 and Strategies for Its Usage in Oxidopyrylium Cycloaddition Chemistry

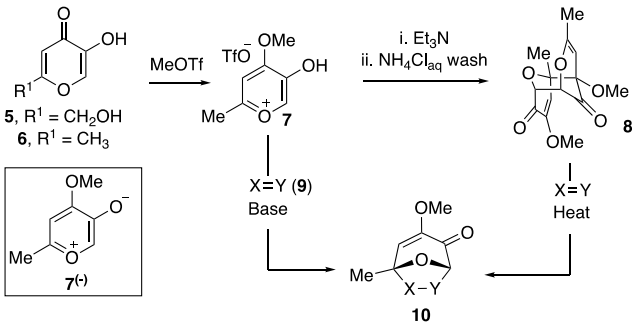

nature. The purification of oxidopyrylium dimer furthermore provides a source of oxidopyrylium ylide free of the Brønsted acid and base and has been advantageous in reaction optimization[6] and total synthesis efforts.[7] However, it should be noted that high temperatures and/or prolonged reaction times are needed, which can present a potential limitation. Thus, understanding how specific structural features influence relative rates of oxidopyrylium ylide dimerization and cycloaddition reactions is of fundamental importance.

Herein, we present experimental and theoretical results on factors that control the dimerization versus cycloaddition behavior of regioisomeric maltol- and allomaltol-derived oxidopyrylium ylides. Specifically, we demonstrate that (i) maltol-derived oxidopyrylium ylide (see $12^{(-)}$ in Scheme 3 for details) is more rapidly trapped by dipolarophiles, such as dimethyl acetylenedicarboxylate (DMAD, **16a**), than the allomaltol-derived ylide ($7^{(-)}$); (ii) density functional theory (DFT) calculations show that homodimerization of maltol-derived oxidopyrylium ylide ($12^{(-)}$ → **13**/**14**, Scheme 3) proceeds through a concerted process, whereas homodimerization of allomaltol-derived oxidopyrylium ylide ($7^{(-)}$ → **8**) proceeds through a two-step process that is lower in energy; (iii) kinetic studies for the reaction between homodimers (**8**/**13**/**14**) and DMAD (**16a**) to form [5 + 2] cycloaddition products reveal different kinetic profiles for the reaction with **8** and that with **13**/**14**, but are each consistent with a mechanism involving full cycloreversion to the oxidopyrylium ylide; and (iv) studies with dipolarophiles are presented to gauge the [5 + 2] cycloaddition trapping efficiencies of the ylides prior to [5 + 3] dimerization.

RESULTS AND DISCUSSION

Initial Observations Illustrating Dramatic Reactivity Differences between Maltol- and Allomaltol-Derived

Scheme 3. Observed Differences of [5 + 2] Cycloadditions of (A) Maltol- and (B) Allomaltol-Derived Oxidopyrylium Salts with Dimethyl Acetylenedicarboxylate (16a)[a−f]

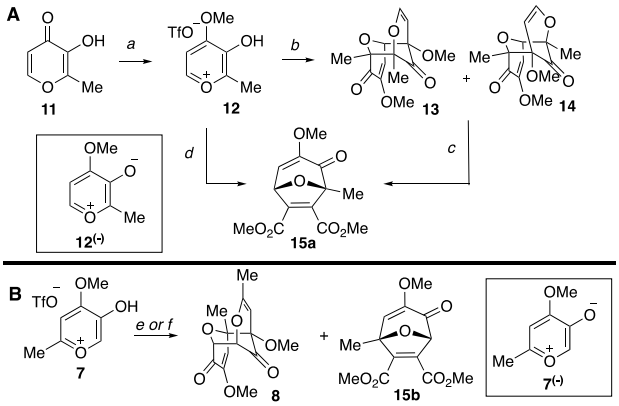

[a]Methyl trifluoromethanesulfonate (1.5 equiv), CH_2Cl_2, reflux, 4 h, 54%. [b]Triethylamine (1.2 equiv), CH_2Cl_2, rt, 2 h, (45% **13**, 25% **14**). [c]Dimethylacetylene dicarboxylate (DMAD, **16a**, 11 equiv), $CDCl_3$, μwave, 150 °C, 2 h, 95% **15a**. [d]DMAD (**16a**, 5 equiv), CD_3CN, then *N*,*N*-diisopropylaniline (1.2 equiv), rt, 30 min, 94% **15a**, 5% **13**/**14**. Yields based on ^{1}H NMR. [e]DMAD (**16a**, 5 equiv), CD_3CN, then *N*,*N*-diisopropylaniline (1.2 equiv), rt, 5 min, 82% **8**, 4% **15b**. Yields based on ^{1}H NMR. [f]*N*,*N*-Diisopropylaniline (1.2 equiv), DMAD (**16a**, 20 equiv), μwave, 100 °C, 5 min, 90% **15b** (see ref 4 for details).

Oxidopyrylium Ylides. Our studies began with an evaluation of maltol-derived oxidopyrylium ylides ($12^{(-)}$, Scheme 3A), which were absent from the literature with the exception of a single report by Li.[8] Upon synthesizing the maltol-derived oxidopyrylium salt (**12**) and treating it to triethylamine, we found that two dimers formed in an approximately 2:1 ratio (**12** → **13** + **14**, Scheme 3A). This result differed from the analogous dimerization of allomaltol-derived salt **7**, which led exclusively to a single isomer, **8** (Scheme 3B). Both dimers **13** and **14** reacted with DMAD (**16a**) at higher temperatures, affording oxidopyrylium cycloaddition product **15a**, confirming that these regioisomeric dimers could be used as a ylide source. However, the reactions were noticeably more sluggish than was expected based on our experience with the analogous reaction with dimer **8**. In fact, the reaction between either dimer **13** or **14** with DMAD (**16a**) only reached ~70% conversion after 8 h at 100 °C as compared to that of full conversion within 5 min with dimer **8** in closely related studies (Scheme 3B).[4] Consistent with these findings, a competition experiment in which a 1:1 mixture of **8** and **13**/**14** heated in the presence of **16a** and monitored over time led first to the formation **15b**, followed by the formation of **15a**. Therefore, to promote a higher-yielding process for the cycloaddition with **13**/**14** and **16a**, the reaction was carried out at elevated temperatures (150 °C), which provided **15a** in a 95% yield after only 2 h (Scheme 3A).

The more sluggish reactivity between dimers **13** and **14** with DMAD (**16a**) was surprising to us, especially in light of findings by Li that a closely analogous reaction between **12** and the presumably less reactive indole was completed within 7 h at room temperature.[8] Upon closer examination, when a CD_3CN solution containing a mixture of oxidopyrylium salt **12** and DMAD (**16a**) was subsequently treated with *N*,*N*-diisopropylaniline, after only 30 min at room temperature, **15a** was the major product, and dimers **13** and **14** were only

DOI: 10.1021/acs.joc.9b02137
J. Org. Chem. 2019, 84, 14670−14678

observed as minor products (**12** → **15a**, Scheme 3A), more closely consistent with the Li studies. The result, however, was highly contradictory to our experience with regioisomeric salt **7**, where dimer **8** is almost always observed as the major product upon the addition of base in the presence of dipolarophiles, and over time or at elevated temperature, it converts to cycloaddition products (**7** → **8** → **15b**, Scheme 3B). Likewise, competition experiments in which a 1:1 mixture of **7** and **12** in the presence of **16a** is treated to *N*,*N*-diisopropylaniline and monitored over time via ^{1}H NMR resulted in only the appearance of dimer **8** (from **7**) and DMAD cycloadduct **15a** (from **12**).

Given these findings, the dimerization processes were evaluated in the absence of DMAD (**16a**). Consistent with prior experiences,[4] the treatment of salt **7** to *N*,*N*-diisopropylaniline led to complete conversion to dimer **8** within 5 min. On the other hand, when salt **12** was treated to identical conditions, conversion to **13** and **14** took upwards of 7 h, and when monitoring the reaction by ^{1}H NMR, no signals were ever observed that could be attributed to ylide $\mathbf{12}^{(-)}$. We initially hypothesized that these slower conversion rates were the result of slower deprotonation, possibly due to an increase in sterics due to the close proximity of the proton to the methyl group of **12**. However, the steric hypothesis was disproven since switching to the less sterically demanding base, *N*,*N*-dimethylaniline, slowed the consumption of **12** even more so, consistent with the lower pK_a of *N*,*N*-dimethylaniline.[9] Likewise, *N*,*N*-dimethylaniline slowed down the conversion of salt **7** to dimer **8** to a rate more comparable with the rate that *N*,*N*-diisopropylaniline promotes the conversion of **12** to **13** and **14** (Scheme 4A). We thus treated a solution of **7** and

Scheme 4. Effects of Base on Salt Conversion and Cycloaddition Trapping Efficiency[a]

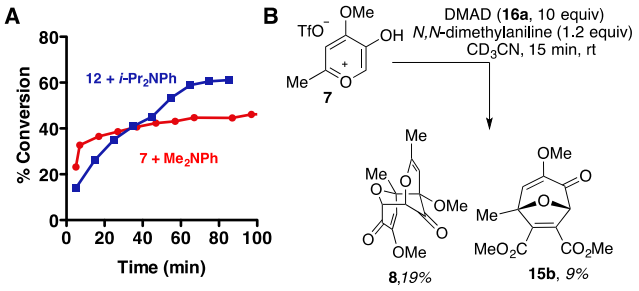

[a](A) Conversion over time of salt **12** with *N*,*N*-diisopropylaniline and salt **7** with *N*,*N*-dimethylaniline. (B) Analysis of the ratio between cycloaddition and dimerization products for the reaction between **7** and DMAD (**16a**) when initiated by *N*,*N*-dimethylaniline, as observed at a partial conversion.

DMAD (**16a**) in CD_3CN to *N*,*N*-dimethylaniline to assess whether greater trapping efficiency could be achieved with slower deprotonation. However, when viewed at only a partial conversion of salt **7** (15 min), dimer **8** remained the major product (Scheme 4B).

The above experimental results made it evident that the differences in DMAD (**16a**) trapping efficiency from salts **7** and **12** prior to dimerization could not be fully explained by simple differences in rates of deprotonation, and thus these differences might exist after the deprotonation step and involve relative reactivities of the ylides. Thus, we turned to DFT calculations to study the relative dimerization and cycloaddition reactions from $\mathbf{7}^{(-)}$ and $\mathbf{12}^{(-)}$.

DFT Calculations. B3LYP/6-31G(d,p) calculations were employed here. Similar DFT calculations have been used to assess the tendency for compounds to dimerize[10] and in cycloadditions of oxidopyrilium ylides.[11] To explore the bimolecular pathways (Scheme 5), we have located structures on the potential energy surface (PES) for the dimerization of maltol $\mathbf{12}^{(-)}$ and allomaltol $\mathbf{7}^{(-)}$ oxidopyrylium ylides. Our calculations focused on the neutral forms of maltol and allomaltol oxidopyrylium ylides since these are expected to give rise to the dimers. Since $\mathbf{7}^{(-)}$ and $\mathbf{12}^{(-)}$ are structural isomers, their relative energies can be readily compared. The global minimum is the complex of $\mathbf{12}^{(-)}$.

Scheme 5A shows the formation of dimer **8** from the allomaltol-derived oxidopyrylium ylide $\mathbf{7}^{(-)}$, which proceeds through a stepwise process. This process involves an initial carbon−carbon bond formation via an aldol-like process between the α-carbon of the embedded enolate of one ylide and the more sterically unencumbered electrophilic carbon of the other. The reaction $\Delta H^{\ddagger}$ is 8.3 kcal/mol (compared to $\mathbf{7}^{(-)}$) and leads to the second step, where a more sterically encumbered carbon creates the second carbon−carbon bond of dimer **8**. In the formation of dimer **8**, there is a methyl−methoxy gauche interaction, but it is lower in energy, likely due to the fact that it is an intermolecular process (TS-2, Figure 1). The formation of dimer **13** from maltol oxidopyrylium ylide $\mathbf{12}^{(-)}$, on the other hand, proceeds through an asynchronous concerted process (Scheme 5B). The dimerization of $\mathbf{12}^{(-)}$ is higher in energy than the dimerization of $\mathbf{7}^{(-)}$ due to an unfavorable methyl−methyl gauche interaction, producing a ∼2 kcal/mol higher transition-state energy (i.e., $\Delta H^{\ddagger}$ of 11.6 kcal/mol) than that of $\mathbf{7}^{(-)}$ (TS-3, Figure 1). An identical $\Delta H^{\ddagger}$ of 11.6 kcal/mol energy barrier exists in the transition state to dimer **14**. Even though sterics of a methoxy group are generally lower in energy than those of a methyl group, this specific methoxy−methyl gauche interaction appears to have added steric strain, where the methyl group of the methoxy extends over the incipient carbonyl group (TS-4, Figure 1). This explains why both dimers of $\mathbf{12}^{(-)}$ are formed, in contrast to the selective [5 + 3] dimerization of $\mathbf{7}^{(-)}$.

The cycloaddition reactions between DMAD (**16a**) and either $\mathbf{7}^{(-)}$ or $\mathbf{12}^{(-)}$ were fairly analogous energetically, and each was predicted to proceed through a concerted, asynchronous pathway. The transition state between DMAD and $\mathbf{12}^{(-)}$ was only slightly favored over that between DMAD and $\mathbf{7}^{(-)}$ (11.7 vs 12.9 kcal/mol, Scheme 1S; see the Supporting Information (SI) section for details). Furthermore, cycloaddition products were thermodynamically favored over dimer products by approximately 40 kcal/mol in both cases, consistent with the observations that, with enough time and energy, all of the dimers investigated can be converted to their respective oxidopyrylium [5 + 2] cycloaddition products.

Kinetic Studies. Kinetic experiments were carried out as a means to evaluate the relative transition-state energy barriers for dimerization and cycloaddition processes. Drawing inspiration and precedence from classic kinetic studies on the reaction between dialkylborane dimers and alkenes by Brown et al.,[12] steady-state approximation was employed to evaluate the reaction between oxidopyrylium dimers (**8**/**13**/**14**) and DMAD (**16a**) (**8** + **16a** → **15b** or **13**/**14** + **16a** → **15a**, Scheme 6). In this way, the kinetics are fixed on the key reactions of interest, namely, the [5 + 2] cycloaddition (k_2)

DOI: 10.1021/acs.joc.9b02137
J. Org. Chem. 2019, 84, 14670−14678

Scheme 5. Computed Potential Energy Surface of Maltol and Allomaltol Oxidopyrylium Ylides $7^{(-)}$ and $12^{(-)}$ [a]

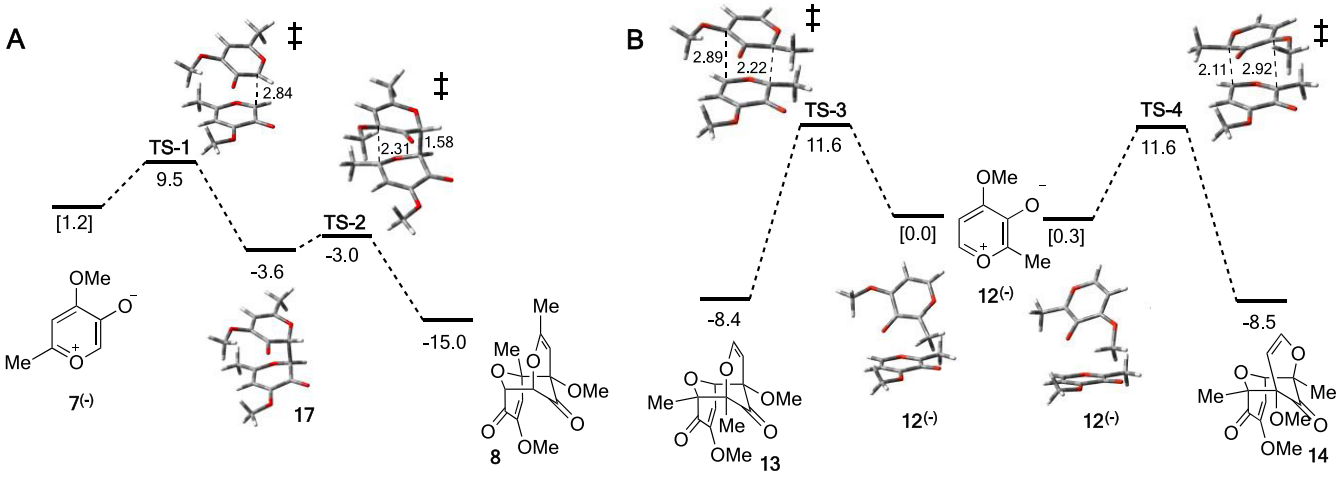

[a]The computed potential surface uses two molecules of $7^{(-)}$ in (A) and two molecules of $12^{(-)}$ in (B).

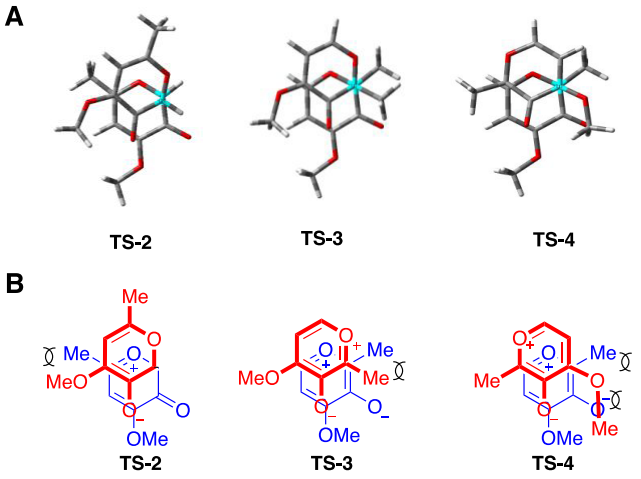

Figure 1. Top perspective of transition states to dimerization to highlight steric interactions. (A) Graphical perspective of the second bond-forming reaction in the production of **8** (TS-2) and the concerted formation of dimers **13** and **14** demonstrating energetically costly steric interactions (TS-3 and TS-4). (B) Transition-state perspectives redrawn and color-coordinated for visual clarity.

Scheme 6. Overview of Competing Cycloaddition and Dimerization Pathways from 7/12, Also Illustrating Conversion of 8/13/14 to 15a/15b

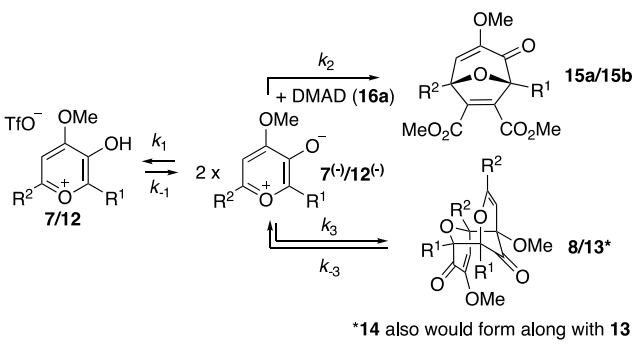

and dimerization/cycloreversion (k_3/k_{-3}) (Scheme 6). Assuming that the energy barrier for the dimerization of $12^{(-)}$ is higher than the energy barrier for the cycloaddition reaction with DMAD (**16a**) to an extent such that $1/2k_2[\mathbf{16a}] \gg k_3[\mathbf{12}^{(-)}]$, the reaction should exhibit first-order kinetics, as represented by the equation $-d[\mathbf{13}]/dt = k_1[\mathbf{13}]$. Conversely, if the cycloaddition step between $7^{(-)}$ and DMAD (**16a**) is higher in energy than the dimerization of $7^{(-)}$ such that $1/2k_2[\mathbf{16a}] \ll k_3[7^{(-)}]$, then the reaction should exhibit three-halves-order kinetics, as represented by the equation $-d[\mathbf{8}]/dt = k_{3/2}[\mathbf{8}]^{1/2}[\mathbf{16a}]$.

To evaluate the kinetics experimentally, the conversion of **8** and **13** was monitored over time with an excess of DMAD (**16a**), and the resultant plots were evaluated for best fit (Figure 2A).[13] Consistent with the anticipated kinetics, the conversion of **8** fits best to half-order kinetics ($[\mathbf{8}]_t^{1/2}$ vs time), whereas the conversion of **13** fits best to first-order kinetics ($\ln[\mathbf{13}]_t$ vs time). We also carried out experiments in the inverse, with an excess of the dimers (Figure 2B). In the

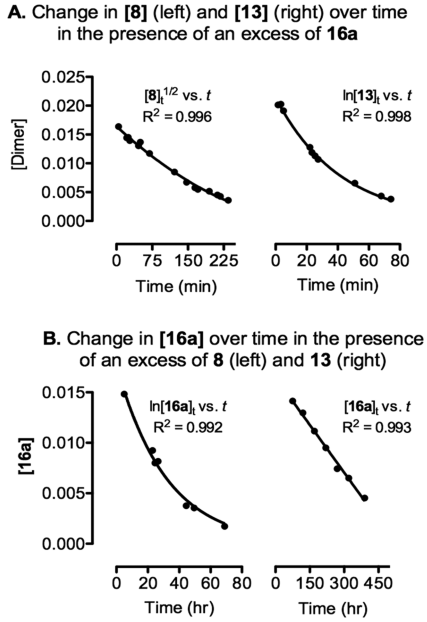

Figure 2. Graphs from kinetics studies. (A) Concentration of dimers **8** and **13** over time with an excess of **16a**. (B) **16a** in an excess of dimers **8** and **13**.

DOI: 10.1021/acs.joc.9b02137
J. Org. Chem. 2019, 84, 14670−14678

presence of dimer **13**, the rate of conversion of DMAD (**16a**) stayed consistent as the concentrations decreased, in line with zero-order kinetics. However, in the presence of dimer **8**, the rate changed as the concentration of DMAD (**16a**) changed, fitting best to first-order kinetics ($\ln[\mathbf{16a}]_t$ vs time). Experiments performed with **14** were also consistent with those performed with **13** (see the Supporting Information). Thus, these studies provided experimental evidence that in the reaction between allomaltol-derived oxidopyrylium ylides $\mathbf{7}^{(-)}$ and **16a**, dimer **8** is the kinetic product, helping explain the difficulty of intercepting $\mathbf{7}^{(-)}$ with DMAD (**16a**). Conversely, the studies also provided experimental evidence that in the reaction between maltol-derived oxidopyrylium ylides $\mathbf{12}^{(-)}$ and **16a**, cycloaddition product **15a** is the kinetic product, which explains why $\mathbf{12}^{(-)}$ can be successfully intercepted with DMAD (**16a**).

Dipolarophile Dependence. Both DFT calculations and kinetic experiments helped explain why DMAD (**16a**) is trapped more efficiently by $\mathbf{12}^{(-)}$ than by $\mathbf{7}^{(-)}$. We next wanted to gauge how their relative trapping efficiency might extend to other dipolarophiles. For these studies, we added *N*,*N*-diisopropylaniline to a solution of CD_3CN containing oxidopyrylium salts **7** and **12** and a panel of dipolarophiles of varying reactivities (**16a**–**d**) and monitored the reaction progress by ^{1}H NMR (Scheme 7). Phenylacetylene (**16d**) is

Scheme 7. Products to Dimer Ratio upon Oxidopyrylium Ylide Formation in the Presence of a Range of Dipolarophiles[a]

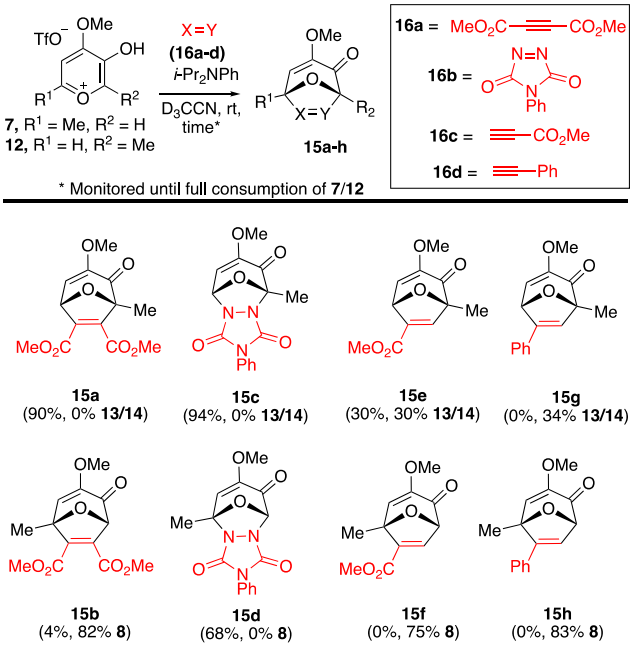

[a]Yields calculated by ^{1}H NMR integration using an internal standard following full consumption of salt.

known to react more sluggishly with $\mathbf{7}^{(-)}$ than DMAD (**16a**).[4] Transition-state energy barriers were thus computed for the reaction of **16d** with $\mathbf{7}^{(-)}$ to form **15g** ($\Delta H^{\ddagger}$ = 16.3 kcal/mol, Scheme 2S; see the SI section for details) and for the reaction of **16d** with $\mathbf{12}^{(-)}$ to form **15h** ($\Delta H^{\ddagger}$ = 17.4 kcal/mol, Scheme 2S; see the SI section for details). As these energy barriers are each higher than their respective dimerization energy barriers, dimerization products should be the kinetic products in both instances. Consistent with this hypothesis, when *N*,*N*-diisopropylaniline was treated to a mixture of **16d** and either salt **7** or **12**, upon complete consumption of salts, only dimerization products were observed (see the entry for products **15g**/**h**).

For a more reactive dipolarophile, we turned to the highly electrophilic 4-phenyl-1,2,4-triazole-3,5-dione (PTAD, **16b**; see the entry for products **15c**/**d**).[14] As anticipated, very low transition-state energy barriers were calculated for the reaction between **16b** and both $\mathbf{7}^{(-)}$ ($\Delta H^{\ddagger}$ = 2.7 kcal/mol) and $\mathbf{12}^{(-)}$ ($\Delta H^{\ddagger}$ = 3.1 kcal/mol, Scheme 3S; see details in the SI section). As these barriers were each substantially lower than those of their respective dimerization reactions, both **15c** and **15d** would be expected to be the kinetic products. Consistent with this, when *N*,*N*-diisopropylaniline was treated to a mixture of **16b** and either salt **7** or **12**, no dimer was observed and the [5 + 2] cycloaddition products **15c** and **15d** predominated. These two sets of experiments demonstrated that with the more extremes on the dipolarophile reactivity spectra, the trapping efficiencies of the two salts are similar. However, when these experiments were performed with the more intermediately reactive dipolarophile, methyl propiolate (**16c**; see the entry for products **15e**/**f**), differences in the trapping efficiencies of $\mathbf{7}^{(-)}$ and $\mathbf{12}^{(-)}$ returned. Specifically, when salt **7** was treated to the base in the presence of **16c**, only dimer **8** was observed, whereas significant amounts of product **15e** were observed in the analogous reaction with **12**.

Mechanistic Interpretation and Implications. Oxidopyrylium ylides $\mathbf{7}^{(-)}$ and $\mathbf{12}^{(-)}$ can undergo both [5 + 3] dimerization and [5 + 2] cycloaddition chemistry to generate dimers (**8**, **13**, **14**) or cycloaddition products (i.e., **15a**/**b**), respectively. The dimerization to **8** and **13**/**14** is reversible and leads back to the ylides, which can then convert further to the thermodynamically stable oxidopyrylium cycloaddition products, **15a** and **15b**, when heated in the presence of DMAD (**16a**). Instead of the dimer reacting directly with the dipolarophile, the kinetic and computational results support a mechanism, whereby dimer conversion to cycloaddition products proceeds through the cycloreversion of the dimers to oxidopyrylium ylides followed by a cycloaddition reaction. Kinetics for these two reactions is different, however. Kinetics from the reaction from dimer **8** and DMAD (**16a**) is consistent with a mechanism wherein the transition-state energy for [5 + 3] cycloreversion/dimerization is lower than that of the [5 + 2] cycloaddition reaction, and that from **13**/**14** consistent with one where the transition state for [5 + 3] cycloreversion/dimerization is higher in energy than that for the [5 + 2] cycloaddition step.

DFT studies were consistent with these trends, revealing that the transition-state barrier for the dimerization of $\mathbf{12}^{(-)}$ is higher in energy than that of $\mathbf{7}^{(-)}$ (Scheme 5), and thus **8** is the kinetic product relative to **15a**, whereas **15b** is the kinetic product relative to **13**/**14**. The DFT studies indicate that these energy differences are the result of unavoidable steric interactions in the transition state toward both dimers **13** and **14**, which alter the mechanism for the different dimerization reactions. The implications to these studies are that by positioning groups ortho to the oxide (e.g., $\mathbf{12}^{(-)}$), the transition-state barrier toward dimerization can increase and improve the success rate of trapping the ylide with a dipolarophile prior to self-dimerization. One could anticipate based upon these results that by increasing the size of these groups, the rate of dimerization will be slowed even further and

DOI: 10.1021/acs.joc.9b02137
J. Org. Chem. 2019, 84, 14670−14678

allow for an even more efficient [5 + 2] trapping. Indeed, 2,4,6-triphenylpyrylium-3-oxide is one of the few oxidopyrylium ylides to ever be observed experimentally and does not dimerize,[15] which may be why it reacts with an extremely broad range of dipolarophiles.[16] In the current studies, dramatic differences in trapping efficiency were observed with DMAD (**16a**) and methyl propiolate (**16c**). However, the more reactive dipolarophile PTAD (**16b**) efficiently intercepted both ylides, whereas the less reactive dipolarophile phenylacetylene (**16d**) could not intercept either ylide. Thus, further structure−activity relationships with a broader range of both oxidopyrylium ylides and dipolarophiles are warranted.

CONCLUSIONS

Synthetic, kinetic, and theoretical approaches have been developed to probe oxidopyrylium ylide reactivity in self-dimerization and cycloaddition reactions. We find the following results: (i) maltol- and allomaltol-derived oxidopyrylium salts serve as precursors to their corresponding oxidopyrylium ylides $7^{(-)}$ and $12^{(-)}$, which themselves serve as intermediates in both self-dimerization and cycloaddition reactions; (ii) DFT calculations provide valuable insight into the dimerization mechanism of these two oxidopyrylium ylides where gauche methyl/methyl or methyl/methoxy interactions favor the dimerization in a kinetically not thermodynamically controlled fashion compared to the [5 + 2] cycloaddition selectivity; (iii) kinetics for the reaction between dimethyl acetylenedicarboxylate (**16a**) and oxidopyrylium dimers suggests that the rate-limiting step with dimer **8** is the cycloaddition reaction; in contrast, the reaction with dimer **13** or **14** is consistent with a mechanism where the rate-limiting step is the cycloreversion to ylide $12^{(-)}$; (iv) while oxidopyrylium ylides $7^{(-)}$ and $12^{(-)}$ have very different trapping efficiency profiles with DMAD (**16a**) and methyl propiolate (**16c**), only cycloaddition products form in the presence of the more reactive PTAD (**16b**), and only dimers form in the presence of less reactive phenylacetylene (**16d**). These studies provide insight into how differences in the structure of the oxidopyrylium ylides such as the placement of appendages can lead to significantly different reactivity behaviors. Future studies combining synthetic, kinetic, and theoretical studies across a broader range of oxidopyrylium ylides should further enhance our understanding of these systems and help inform future synthetic strategies employing oxidopyrylium cycloaddition and dimerization reactions. For example, the decomposition of homodimers is a retro reaction of "masked" neutral oxidopyrylium ylide monomers and is a base-free strategy that could be valuable for some reactions. In contrast to the reactivity of DMAD with dimers **8**, **13**, and **14**, Hendrickson's early work described how the reaction between the dimer of an unsubstituted 3-oxidopyrylium ylide and DMAD only forms trace products, even at 200 °C.[2b] Thus, there appear to be structural advantages to dimers **8**, **13**, and **14** that allow them to behave as oxidopyrylium ylide sources. It seems reasonable to hypothesize that the OMe plays an important role in this reactivity by both enhancing the nucleophilicity of the ylides and destabilizing the ground state of **8** and **14** through the gauche interactions it presents. Further studies are underway to assess the importance of the OMe group for efficient dimerization reversibility and whether other oxidopyrylium ylide dimers without OMe groups may also behave as ylide sources. In other instances, dimerization may pose greater technical challenges, and knowledge of how to effectively trap out ylides prior to dimerization will be valuable.

EXPERIMENTAL SECTION

General Information. All starting materials and reagents were purchased from commercially available sources and used without further purification, with the exception of CH_2Cl_2, which was purified on a solvent purification system prior to reactions. ^1H and ^{13}C NMR shifts were measured using the solvent residual peak as the internal standard and reported as follows: chemical shift, multiplicity (s = singlet, bs = broad singlet, d = doublet, t = triplet, dd = doublet of doublets, q = quartet, m = multiplet), coupling constant (Hz), integration. Infrared (IR) spectral bands are characterized as broad (br), strong (s), medium (m), and weak (w). Mass spectra were recorded on a spectrometer by the electrospray ionization (ESI) technique with a time-of-flight (TOF) mass analyzer. Microwave reactions were performed via the Biotage Initiator EXP US (manufacturer #: 355302) (external IR temperature sensor) in a sealed vessel. Where noted, reaction products were purified via silica gel chromatography using a Biotage Isolera Prime, with Biotage SNAP Ultra 10 g or 25 g cartridges, in a solvent system of ethyl acetate (EtOAc) in hexane.

Synthesis and Characterization of Maltol-Derived Oxidopyrylium Salt. *3-Hydroxy-4-methoxy-2-methylpyrylium Trifluoromethanesulfonate (**12**).* To a solution of maltol (**11**, 5 g, 0.0396 mol) in CH_2Cl_2 (10 mL) was added methyl trifluoromethanesulfonate (MeOTf, 6.5 mL, 0.0594 mol). The reaction was allowed to stir at reflux for 4 h, cooled to an ambient temperature, and then evaporated under reduced pressure to yield **12** as solid white crystals (6.5 g, 54% yield), with a melting point range of 99−102 °C. IR (thin film, KBr): 3088 (w), 1634 (s), 1554 (w), 1497 (m), 1438 (w), 1258 (b), 1164 (s), 1069 (w), 1033 (s), 962 (w), 903 (w), 827 (w), 750 (b), 636 (s) cm^{-1}. ^1H NMR (400 MHz, CD_3CN) δ 8.80 (d, J = 5.2 Hz, 1H), 7.60 (d, J = 5.2 Hz, 1H), 4.31 (s, 3H), 2.68 (s, 3H). $^{13}C\{^1H\}$ NMR (101 MHz, CD_3CN) δ 168.8, 166.4, 161.2, 142.9, 108.5, 60.7, 16.3.

Synthesis and Characterization of Maltol-Derived Oxidopyrylium Dimers (13) and (14). In a round-bottom flask, triflate salt **12** (0.1 g, 0.345 mmol, 1 equiv) was suspended in CH_2Cl_2 (3 mL, 0.1 M). Triethylamine (96 μL, 0.690 mmol, 2 equiv) was slowly added to the reaction mixture, at which time the solid slowly dissolved. The reaction mixture was allowed to stir for 2 h at room temperature and then quenched with saturated aqueous ammonium chloride (5 mL). The organic layer was isolated, and the aqueous layer was extracted with CH_2Cl_2 (3 × 10 mL). The combined organics were dried over Na_2SO_4, filtered, and concentrated under reduced pressure. The crude material was purified by chromatography (Biotage Isolera Prime, SNAP 12 g silica gel, 18 cm × 1.8 cm, solvent gradient: 0−25% EtOAc in hexanes (500 mL)). Two products were separated, and product fractions were concentrated to yield **13** (22 mg, 0.0786, 45% yield) and **14** (12 mg, 0.0429, 25% yield), both isolated as white solids.

*(±)-(1R,2S,6S,7R)-6,9-Dimethoxy-1,2-dimethyl-3,11-dioxatricyclo[5.3.1.1^{2,6}]dodeca-4,8-diene-10,12-dione (**13**).* Mp: 129−132 °C. R_f = 0.14 in 20% ethyl acetate in hexanes. IR (ATR, ZnSe) 3090 (w), 3002 (w), 2941 (br), 2834 (br), 1742 (s), 1699 (s), 1626 (s), 1455 (w), 1358 (m), 1258 (m), 1170 (s), 1139 (s), 1066 (s), 1036 (m), 914 (m), 841 (w), 789 (w). ^1H NMR (400 MHz, $CDCl_3$) δ 6.67 (d, J = 5.9 Hz, 1H), 6.01 (d, J = 5.1 Hz, 1H), 5.02 (d, J = 5.9 Hz, 1H), 4.49 (d, J = 5.1 Hz, 1H), 3.63 (s, 3H), 3.49 (s, 3H), 1.55 (s, 3H), 1.25 (s, 3H). $^{13}C\{^1H\}$ NMR (101 MHz, $CDCl_3$) δ 199.5, 188.8, 149.9, 148.2, 113.0, 100.5, 92.4, 87.6, 86.3, 77.4, 55.5, 54.1, 17.3, 14.7. HRMS (ESI-TOF) m/z: $[M + H]^+$ calcd for $C_7H_9O_3^+$: 141.0473. Found: 141.0561.

*(±)-(1R,2R,6R,7R)-6,9-Dimethoxy-2,7-dimethyl-3,11-dioxatricyclo[5.3.1.1^{2,6}]dodeca-4,9-diene-8,12-dione (**14**).* Mp: 159−159 °C. R_f = 0.14 in 25% ethyl acetate. IR (ATR, ZnSe) 3090 (w), 3002 (w), 2941 (br), 2834 (br), 1742 (s), 1699 (s), 1626 (s), 1455 (w), 1358 (m), 1258 (m), 1170 (s), 1139 (s), 1066 (s), 1036 (m), 914 (m), 841 (w), 789 (w). ^1H NMR (400 MHz, $CDCl_3$) δ 6.69

DOI: 10.1021/acs.joc.9b02137
J. Org. Chem. 2019, 84, 14670−14678

(d, J = 6.0 Hz, 1H), 5.64 (d, J = 5.2 Hz, 1H), 4.92 (d, J = 6.0 Hz, 1H), 4.74 (d, J = 5.2 Hz, 1H), 3.60 (s, 3H), 3.43 (s, 3H), 1.45 (s, 3H), 1.39 (s, 3H). $^{13}C\{^1H\}$ NMR (101 MHz, $CDCl_3$) δ 199.3, 188.5, 150.7, 148.3, 109.0, 98.3, 89.7, 87.8, 86.0, 80.0, 55.4, 54.5, 17.1, 17.0. HRMS (ESI-TOF) m/z: $[M + H]^+$ calcd for $C_7H_9O_3^+$: 141.0473. Found: 141.0838. Stereochemistry of **13** and **14** was determined by X-ray crystal analysis. See X-ray section, below, for details.

Synthesis of New Oxidopyrylium [5 + 2] Cycloadducts for Characterization. Cycloadducts **15b**, **15f**, and **15h** were synthesized previously.[4] Compounds **15a, 15c, 15d, 15e**, and **15g** were synthesized as follows to provide characterization data in support of ^1H NMR yields described in Scheme 7.

*(±)-Dimethyl (1S,5S)-3-Methoxy-5-methyl-4-oxo-8-oxabicyclo-[3.2.1]octa-2,6-diene-6,7-dicarboxylate (**15a**).* To a solution of **13/14** (20 mg, 0.0714 mmol, 1 equiv) in $CDCl_3$ (1 mL, 0.9 M) was added dimethyl acetylenedicarboxylate (**16a**, 100 μL, 0.814 mmol, 11 equiv). The reaction was subjected to microwave irradiation at 150 °C for 2 h and immediately purified by chromatography (Biotage Isolera Prime, SiliCycle SiliaSep 25 g silica gel, 40−63 μm 60 Å, solvent gradient: 0−25% EtOAc in hexanes (500 mL)). Product fractions were concentrated in vacuo to yield **15a** as a pale, yellow oil (38 mg, 95% yield). R_f = 0.53 in 25% ethyl acetate. IR (thin film, KBr): 2956 (w), 2843 (w), 1716 (s), 1654 (w), 1614 (m), 1438 (m), 1379 (w), 1281 (b), 1146 (w), 1069 (s), 1005 (m), 933 (w), 902 (w), 878 (w), 847 (w), 812 (w), 787 (w), 766 (w), 700 (w), 6309 (w) cm^{-1}. ^1H NMR (400 MHz, $CDCl_3$) δ 6.15 (d, J = 4.9 Hz, 1H), 5.39 (d, J = 4.9 Hz, 1H), 3.79 (d, J = 6.4 Hz, 6H), 3.56 (s, 3H), 1.59 (s, 3H). $^{13}C\{^1H\}$ NMR (101 MHz, $CDCl_3$) δ 188.2, 163.1, 162.1, 146.5, 146.4, 143.1, 114.4, 94.0, 78.2, 55.1, 52.8. 52.8, 16.2. HRMS (ESI-TOF) m/z: $[M + H]^+$ calcd for $C_{13}H_{15}O_7^+$: 283.0812. Found: 283.0817.

*(±)-(5R,9S)-7-Methoxy-5-methyl-2-phenyl-1H,5H-5,9-epoxy-[1,2,4]triazolo[1,2-a][1,2]diazepine-1,3,6(2H,9H)-trione (**15c**).* To a solution of **12** (50 mg, 0.172 mmol, 1 equiv) and 4-phenyl-1,2,4-triazole-3,5-dione (**16b**, 60 mg, 0.344 mmol, 2 equiv) in CD_3CN (600 μL, 0.3 M) was added *N,N*-diisopropylaniline (29 μL, 0.2068 mmol, 1.2 equiv). The reaction was stirred for 5 min and then immediately purified by chromatography (Biotage Isolera Prime, SiliCycle, SiliaSep 25 g silica gel column, 40−63 μm 60 Å, solvent gradient: 0−25% EtOAc in hexanes (500 mL)). Product fractions were concentrated in vacuo to yield **12** as a white solid (39 mg, 72% yield). Mp: 65−70 °C. R_f = 0.50 in 25% in ethyl acetate. IR (thin film, KBr): 3429 (br), 1731 (s), 1633 (w), 1498 (w), 1399 (m), 1363 (w), 1232 (w), 1148 (w), 1075 (m), 778 (w), 690 (w) cm^{-1}. ^1H NMR (400 MHz, $CDCl_3$) δ 7.51−7.38 (m, 5H), 6.34 (d, J = 5.0 Hz, 1H), 6.11 (d, J = 5.0 Hz, 1H), 3.70 (s, 3H), 1.96 (s, 3H).$^{13}C\{^1H\}$ NMR (101 MHz, $CDCl_3$) δ 182.2, 156.5, 154.87, 150.9, 130.9, 129.5, 129.1, 125.6, 109.8, 96.8, 83.4, 55.9, 15.2. HRMS (ESI-TOF) m/z: $[M + H]^+$ calcd for $C_{15}H_{14}N_3O_5^+$: 316.0928. Found: 316.0928.

*Synthesis of (5R,9S)-7-Methoxy-9-methyl-2-phenyl-1H,5H-5,9-epoxy[1,2,4]triazolo[1,2-a][1,2]diazepine-1,3,6(2H,9H)-trione (**15d**) in the Presence of Excess Salt[a].* To a mixture of oxidopyrylium salt **12** (20 mg, 0.0689 mmol) and 4-phenyl-1,2,4-triazoline-3,5-dione (**16b**, 8 mg, 0.0457 mmol) in dichloromethane (1 mL, 0.0457 M) was added triethylamine (12 μL, 0.0860 mmol). The reaction was stirred for 5 min at room temperature and subsequently washed with aqueous ammonium chloride (3 × 3 mL). The organic layer was isolated, and the aqueous layer was extracted with CH_2Cl_2 (3 × 5 mL). The combined organic layers were dried over Na_2SO_4, filtered, and concentrated under reduced pressure to yield a mixture of dimer **8**, cycloadduct **15d**, and PTAD (**16b**). **15d** is unstable to chromatography, and attempts at crystallization were unsuccessful. It was thus characterized as a mixture of the three. See the Supporting Information for further details. ^1H NMR (400 MHz, CD_3CN) δ 7.59−7.35 (m, Ar)[a], 6.28 (s, 1H), 5.86 (s, 1H), 3.66 (s, 3H), 2.07 (s, 3H). $^{13}C\{^1H\}$ NMR (101 MHz, $CDCl_3$) δ 182.5, 157.3, 155.8, 150.5, 125−135 (Ar),[a] 116.6, 89.9, 56.5, 55.3, 21.1. HRMS (ESI-TOF) m/z: $[M + H]^+$ calcd for $C_{15}H_{14}N_3O_5^+$: 316.0928. Found: 316.0928.

*(±)-Methyl (1S,5S)-3-Methoxy-1-methyl-2-oxo-8-oxabicyclo-[3.2.1]octa-3,6-diene-6-carboxylate (**15e**).* To a solution of **14** (25 mg, 0.0893 mmol, 1 equiv) in $CDCl_3$ (1 mL, 0.9 M) was added methyl propiolate (**16c**, 80 μL, 0.893 mmol, 10 equiv). The reaction was subjected to microwave irradiation at 100 °C for 2 h and then purified by chromatography (Biotage Isolera Prime, SiliCycle SiliaSep 25 g silica gel column, 40−63 μm 60 Å, solvent gradient: 0−25% EtOAc in hexanes (500 mL)). Product fractions were concentrated in vacuo to yield **15e** as a yellow oil (18 mg, 60% yield). R_f = 0.20 in 25% ethyl acetate. IR (thin film, KBr): 3448 (br), 2956 (w), 2358 (w), 1716 (s), 1654 (w), 1614 (m), 1438 (m), 1336 (m), 1379 (w), 1227 (w) 1281 (br), 1146 (w), 1069 (s), 1033 (m), 933 (w), 902 (w), 878 (w), 847 (w), 812 (w) cm^{-1}. ^1H NMR (400 MHz, $CDCl_3$) δ 6.88 (s, 1H), 6.22 (d, J = 4.9 Hz, 1H), 5.41 (d, J = 4.9 Hz, 1H), 3.81 (s, 3H), 3.57 (s, 3H), 1.59 (s, 3H). $^{13}C\{^1H\}$ NMR (101 MHz, $CDCl_3$) δ 190.6, 163.1, 148.2, 146.5, 142.2, 115.6, 93.5, 78.1, 55.0, 52.4, 17.1. HRMS (ESI-TOF) m/z: $[M + H]^+$ calcd for $C_{11}H_{13}O_5^+$: 225.0757. Found: 225.0751.

*(±)-(1S,5S)-3-Methoxy-1-methyl-6-phenyl-8-oxabicyclo[3.2.1]-octa-3,6-dien-2-one (**15g**).* To a solution of **14** (25 mg, 0.0893 mmol, 1 equiv) in $CDCl_3$ (1 mL, 0.9 M) was added phenylacetylene (**16d**, 100 μL, 0.911 mmol, 11 equiv). The reaction was subjected to microwave irradiation at 120 °C for 8 h and then purified by chromatography (Biotage Isolera Prime, SiliCycle SiliaSep 25 g silica gel column, 40−63 μm 60 Å, solvent gradient: 0−25% EtOAc in hexanes (500 mL)). Product fractions were concentrated in vacuo to yield **14** as a yellow oil (7 mg, 16% yield). R_f = 0.13 in 25% in ethyl acetate. IR (thin film, KBr): 3446 (br), 2933 (w), 1705 (s), 1614 (m), 1446 (w), 1343 (w), 1242 (w), 1063 (br), 905 (w), 852 (w), 691 (w), 649 (w) cm^{-1}. ^1H NMR (400 MHz, $CDCl_3$) δ 7.42−7.35 (m, 5H), 6.30 (d, J = 4.9 Hz, 1H), 6.27 (s, 1H), 5.58 (d, J = 4.8 Hz, 1H), 3.55 (s, 3H), 1.63 (s, 3H). $^{13}C\{^1H\}$ NMR (101 MHz, $CDCl_3$) δ 191.6, 155.8, 147.4, 131.9, 129.4, 129.1, 126.0, 124.0, 114.9, 93.1, 79.1, 55.0, 17.6. HRMS (ESI-TOF) m/z: $[M + H]^+$ calcd for $C_{15}H_{15}O_3^+$: 243.1016. Found: 243.1001.

Evaluation of Product versus Dimer Upon Full Conversion of Oxidopyrylium Salt. In a small vial containing salt (**7** or **12**) (5 mg, 0.0172 mmol, 1 equiv) and alkyne (**16a−d**) (0.172 mmol, 10 equiv) in 600 μL of CD_3CN was added *N,N*-diisopropylaniline (4 μL, 0.0207 mmol, 1.2 equiv). The reaction was monitored over time by ^1H NMR, and yields were calculated using ^1H NMR integration based upon the known amount of 3,5-di-*tert*-butyltoluene standard in the reaction mixture. For conversion to known compounds **15b**, **15f**, **15h**, and **8**, ^1H NMR of reactions was compared to literature spectra.[4]

Rate Studies. All rate studies were conducted in Wilmad low-pressure/vacuum NMR tube where concentrations of substrates were determined via the known amount of added internal NMR standard, 3,5-di-*tert*-butyltoluene. For conversion to known compound **15b**, ^1H NMR spectra were compared to literature spectra.[4] All experiments were run at least twice to obtain consistent data sets.

*General Procedure for Excess of **16a** with Dimers **8, 13, and 14** Separately.* To dimer (**8**, **13**, or **14**) (3 mg, 0.01 mmol) in 600 μL of deuterated toluene was added **16a** (26.5 μL, 0.2 mmol, 20 equiv). The reaction was heated in an oil bath (100 °C for dimers **13** and **14**, 70 °C for dimer **8**) and monitored to near completion via internal NMR standard (3,5-di-*tert*-butyltoluene).

*General Procedure for Excess of Dimers **8, 13, and 14** Separately with **16a**.* To dimer (**8**, **13**, or **14**) (15 mg, 0.05 mmol) in 600 μL of deuterated toluene was added **16a** (1.3 μL, 0.01 mmol). The reaction was heated in an oil bath (100 °C for dimers **13** and **14**, 70 °C for dimer **8**) and monitored to near completion via internal NMR standard (3,5-di-*tert*-butyltoluene).

Computational Methods. Optimizations, frequency calculations, and the intrinsic reaction coordinate calculations were performed with Gaussian 09 (revision D.01)[17] at the B3LYP/6-31G(d,p) level of theory[18] and visualized with Gaussview 5.0.[19] These calculations yielded results in reasonably good agreement with the experiment. The energetics are reported as the thermal enthalpies. For the potential energy surface (PES) in Scheme 5, frequency calculations established the nature of the stationary point obtained. Vibrational analyses showed that TS-1−TS-4 species were transition structures, while $7^{(-)}$, **8**, $\mathbf{12}^{(-)}$, **13**, and **17** minima. The intrinsic reaction

DOI: 10.1021/acs.joc.9b02137
J. Org. Chem. 2019, 84, 14670−14678

coordinate[20] calculations were used to verify the transition structures TS-1−TS-4.

X-ray. The structures of **8**, **13**, and **14** are the first to be determined for these tricyclic heterocycles, and they confirm the proposed structures. Crystals were grown using the vapor diffusion technique, using minimal ethyl acetate to solubilize dimers and hexanes as the outer solvent. The crystals of **13** and **14** appeared to be split crystals, most likely with more than two domains, giving rise to relatively high residuals due to overlapping peaks, and in addition, **13** was not strongly diffracting. The X-ray intensity data were measured on a Bruker Smart Breeze CCD system equipped with a graphite monochromator at 100(2) K and cooled by an Oxford Cryosystems 700 Series Cryostream. A total of 1464 frames were collected and integrated with the Bruker SAINT software package, using a narrow-frame algorithm. Data were corrected for absorption effects using the multiscan method (SADABS or TWINABS). The structures were solved and refined using the Bruker SHELXTL software package. All data and methods may be found in the cif files included in the Supporting Information. Briefly, the refinement of **8** was routine, and **13** was refined as a two-component twin. Compound **14** had to be refined as a two-component twin but the second domain refined to just 2% and also exhibited a ∼1:1 disorder for molecule 2 of the two in the asymmetric unit, for one methoxy−methyl and one methyl group.

Cambridge Crystallographic Data Centre deposition numbers for **8**, **13**, and **14**: CCDC 1935838, 1935839, and 1935840.

■ ASSOCIATED CONTENT

Supporting Information

The Supporting Information is available free of charge on the ACS Publications website at DOI: 10.1021/acs.joc.9b02137.

Crystallographic data for compound **8** (CIF)

Crystallographic data for compound **13** (CIF)

Crystallographic data for compound **14** (CIF)

^{1}H and ^{13}C NMR spectra of all new compounds, a discussion on the characterization of **15d** as a mixture, including ^{1}H and ^{13}C NMR data of PTAD (**16d**) and dimer **8**, graphs used to determine kinetic rate data, DFT computed data, and X-ray data for **8**, **13**, and **14** (PDF)

■ AUTHOR INFORMATION

Corresponding Authors

*E-mail: edyta.greer@baruch.cuny.edu (E.M.G.).

*E-mail: rpmurelli@brooklyn.cuny.edu (R.P.M.).

ORCID

Alexander Greer: 0000-0003-4444-9099

William H. Hersh: 0000-0002-9129-3464

Edyta M. Greer: 0000-0003-4283-0523

Ryan P. Murelli: 0000-0002-4247-3936

Notes

The authors declare no competing financial interest.

■ ACKNOWLEDGMENTS

L.P.B., A.K.G., D.M.S., and R.P.M. acknowledge support from the National Institutes of Health (SC1GM111158). E.M.G. acknowledges support from the donors of the Petroleum Research Fund of the American Chemical Society. A.G. acknowledges support from the National Science Foundation (CHE-1856765). This work used Comet, the Extreme Science and Engineering Discovery Environment (XSEDE) cluster at the San Diego Supercomputer Center, which is supported by the National Science Foundation grant number ACI-1548562 through allocation CHE-180060. The authors also thank PSC-CUNY for funding.

■ ADDITIONAL NOTE

[a]For compound **15d**, aromatic regions are undefined due to the presence of PTAD overlapping in the aromatic region. See supporting information for further details.

■ REFERENCES

(1) For some lead examples, see: (a) Hendrickson, J. B.; Farina, J. S. A New 7-Ring Cycloaddition Reaction. *J. Org. Chem.* **1980**, *45*, 3359−3361. (b) Sammes, P. G.; Street, L. J. Intramolecular Cycloadditions with Oxidopyrylium Ylides. *J. Chem. Soc., Chem. Commun.* **1982**, 1056−1057. (c) Mei, G.; Liu, X.; Quao, C.; Chen, W.; Li, C.-C. Type II Intramolecular [5 + 2] Cycloaddition: Facile Synthesis of Highly Functionalized Bridged Ring Systems. *Angew. Chem., Int. Ed.* **2015**, *54*, 1754−1758. (d) Liu, J.-Y.; Wu, J.-L.; Fan, J.-H.; Yan, X.; Mei, G.; Li, C.-C. Asymmetric Total Synthesis of Cyclotrinol. *J. Am. Chem. Soc.* **2018**, *140*, 5365−5369. (e) Liu, X.; Liu, J.-Y.; Wu, J.-L.; Huang, G.-C.; Liang, R.; Chung, L.-W.; Li, C.-C. Asymetric Total Synthesis of Cerorubenic Acid-III. *J. Am. Chem. Soc.* **2019**, *141*, 2872−2877. (f) Nicolaou, K. C.; Kang, Q.; Ng, S. Y.; Chen, D. Y.-K. Total Synthesis of Englerin A. *J. Am. Chem. Soc.* **2010**, *132*, 8219−8222. (g) Snider, B. B.; Wu, X.; Nakamura, S.; Hashimoto, S. A Short Biomimetic Synthesis of (±)-Polygalolides A and B. *Org. Lett.* **2007**, *9*, 873−874. (h) Wender, P. A.; Mascareñas, J. L. Studies on Tumor Promoters. 11. A New [5+2] Cycloaddition Method and its Application to the Synthesis of BC Ring Precursors of Phorboids. *J. Org. Chem.* **1991**, *56*, 6267−6269. (i) Zhao, C.; Glazier, D. A.; Yang, D.; Yin, D.; Guzel, I. A.; Aristov, M. M.; Liu, P.; Tang, W. Intermolecular Regio- and Stereoselective Hetero-[5 + 2] Cycloaddition of Oxidopyrylium Ylides and Cyclic Imines. *Angew. Chem., Int. Ed.* **2019**, *58*, 887−891. (j) Tchabanenko, K.; McIntyre, P.; Malone, J. F. Rapid Annulation of Tropolone Units via a Pyrylium Ylide 1,3-Dipolar Cycloaddition Reaction. *Tetrahedron Lett.* **2010**, *51*, 86−88. (k) Adlington, R. M.; Baldwin, J. E.; Mayweg, A. V. W.; Pritchard, G. J. Biomimetic Cycloaddition Approach to Tropolone Natural Products via an Ortho-Quinone Methide. *Org. Lett.* **2002**, *4*, 3009−3011. (l) Suga, H.; Iwai, T.; Shimizu, M.; Takahashi, K.; Toda, Y. Efficient Generation of an Oxidopyrylium Ylide using a Pd Catalyst and its [5+2] Cycloadditions with Several Dipolarophiles. *Chem. Commun.* **2018**, *54*, 1109−1112. (m) Magnus, P.; Shen, L. Stereoselective Synthesis of the "Cyathin" Diterpene Skeleton via an Intramolecular Pyrylium Ylide-Alkene cyclization. *Tetrahedron* **1999**, *55*, 3553−3560. (n) Woodall, E. L.; Simanis, J. A.; Hamaker, C. G.; Goodell, J. R.; Mitchell, T. A. Unique Reactivity of anti- and syn-Acetoxypyranones en Route to Oxidopyrylium Intermediates Leading to a Cascade Process. *Org. Lett.* **2013**, *15*, 3270−3273. For reviews, see: (o) Bejcek, L. P.; Murelli, R. P. Oxidopyrylium [5 + 2] Cycloaddition Chemistry: Historical Perspective and Recent Advances (2008−2018). *Tetrahedron* **2018**, *74*, 2501−2521. (p) Singh, V.; Krishna, U. M.; Vikrant; Trivedi, G. K. Cycloaddition of Oxidopyrylium Species in Organic Synthesis. *Tetrahedron* **2008**, *64*, 3405−3428. (q) Ylijoki, K. E. O.; Stryker, J. M. [5 + 2] Cycloaddition Reactions in Organic and Natural Product Synthesis. *Chem. Rev.* **2013**, *113*, 2244−2266.

(2) (a) Lee, H.-Y.; Kim, H.-Y.; Kim, B. G.; Kee, J. M. The Stereoselective Dimerization Reaction of Oxidopyrylium Ions. *Synthesis* **2007**, *15*, 2360−2364. (b) Hendrickson, J. B.; Farina, J. S. A simple synthesis of 8- and 10-membered carbocyclic rings. *J. Org. Chem.* **1980**, *45*, 3361−3363.

(3) Wender, P. A.; Mascareñas, J. L. Preparation and Cycloadditions of a 4-Methoxy-3-oxidopyrylium Ylide: A Reagent for the Synthesis of Highly Substituted 7-Membered Rings and Tetrahydrofurans. *Tetrahedron Lett.* **1992**, *33*, 2115−2118.

(4) Meck, C.; Mohd, N.; Murelli, R. P. An Oxidopyrylium Cyclization/ Ring-Opening Route to Polysubstituted α-Hydroxytropolones. *Org. Lett.* **2012**, *14*, 5988−5991.

DOI: 10.1021/acs.joc.9b02137
J. Org. Chem. 2019, 84, 14670−14678

(5) D'Erasmo, M. P.; Murelli, R. P. Fluorous-Phase Approach to α-Hydroxtropolone Synthesis. *J. Org. Chem.* **2018**, *83*, 1478−1485.
(6) (a) D'Erasmo, M. P.; Masaoka, T.; Wilson, J. A.; Hunte, E. M., Jr.; Beutler, J. A.; Le Grice, S. F. J.; Murelli, R. P. Traceless Solid-Phase α-Hydroxtropolone Synthesis. *MedChemComm* **2016**, *9*, 1789−1792. (b) Fuhr, K. N.; Hirsch, D. R.; Murelli, R. P.; Brenner-Moyer, S. E. Catalytic Enantioselective Intermolecular [5 + 2] Dipolar Cycloadditions of a 3-Hydroxy-4-Pyrone-Derived Oxidopyrylium Ylide. *Org. Lett.* **2017**, *19*, 6356−6359.
(7) Hirsch, D. R.; Schiavone, D. V.; Berkowitz, A. J.; Morrison, L. A.; Masaoka, T.; Wilson, J. A.; Lomonosova, E.; Zhao, H.; Patel, B. S.; Dalta, S. H.; Majidi, S. J.; Pal, R. K.; Gallicchio, E.; Tang, L.; Tavis, J. E.; Le Grice, S. F. J.; Beutler, J. A.; Murelli, R. P. Synthesis and Biological Assessment of 3,7-Dihydroxytropolones. *Org. Biomol. Chem.* **2018**, *16*, 62−69.
(8) (a) Mei, G.; Yuan, H.; Gu, Y.; Chen, W.; Chung, L. W.; Li, C.-C. Dearomative Indole [5 + 2] Cycloaddition Reactions: Stereoselective Synthesis of Highly Functionalized Cyclohepta[b]indoles. *Angew. Chem., Int. Ed.* **2014**, *53*, 11051−11055. (b) For studies on cycloaddition chemistry directly from salt **12**, see: Mascareñas, J. L.; Perez, I.; Rumbo, A.; Castedo, L. A New [5 + 2] Annulation Method for the Synthesis of 8-oxabicyclo[3.2.1]octanes from Pyrones. *Synlett* **1997**, *1*, 81−82.
(9) Measured pK_a of *N,N*-diisopropylaniline and *N,N*-dimethylaniline are 7.4 and 5.12, respectively. See: Adams, D. J.; Johns, B.; Vedernikov, A. N. Methyl Transfer Reactivity of Pentachloromethylplatinate(IV) Anion with a Series of *N*-Nucleophiles. *J. Organomet. Chem.* **2019**, *880*, 22−28.
(10) (a) Voloshchuk, T.; Farina, N. S.; Wauchope, O. R.; Kiprowska, M.; Haberfield, P.; Greer, A. Molecular Bilateral Symmetry of Natural Products: Prediction of Selectivity of Dimeric Molecules by Density Functional Theory and Semiempirical Calculations. *J. Nat. Prod.* **2004**, *67*, 1141−1146. (b) Greer, A.; Wauchope, O. R.; Farina, N. S.; Haberfield, P.; Liebman, J. F. Paradigms and Paradoxes: Mechanisms for Possible Enhanced Biological Activity of Bilaterally Symmetrical Chemicals. *Struct. Chem.* **2006**, *17*, 347−350.
(11) (a) Burns, J. M.; Boittier, E. D. Pathway Bifurcation in the [4 + 3]/[5 + 2]-Cycloaddition of Butadiene and Oxidopyrylium Ylides: The Significance of Molecular Orbital Isosymmetry. *J. Org. Chem.* **2019**, *84*, 5997−6005. (b) Kaufman, R. H.; Law, M. C.; Simanis, J. A.; Woodall, E. L.; Zwick, C. R., III; Wedler, H. B.; Wendelboe, P.; Hamaker, C. G.; Goodell, J. R.; Tantillo, D. J.; Mitchell, T. A. Oxidopyrylium-Alkene [5 + 2] Cycloaddition Conjugate Addition Cascade (C3) Sequences: Scope, Limitation, and Computational Investigations. *J. Org. Chem.* **2018**, *83*, 9818−9838. (c) Kuthanapillil, J. M.; Nijamudheen, A.; Joseph, N.; Prakash, P.; Suresh, E.; Datta, A.; Radhakrishnan, K. V. Cycloaddition of Pentafulvenes with 3-Oxidopyrylium Betaine: Experimental and Theoretical Investigations. *Tetrahedron* **2013**, *69*, 9751−9760.
(12) Brown, H. C.; Wang, K. K.; Scouten, C. G. Hydroboration Kinetics: Unusual Kinetics for the Reaction of 9-Borabicyclo[3.3.1]-nonane with Representative Alkenes. *Proc. Natl. Acad. Sci. U.S.A.* **1980**, *77*, 698−702.
(13) Meek, S. J.; Pitman, C. L.; Miller, A. J. M. Deducing Reaction Mechanism: A Guide for Students, Researchers, and Instructors. *J. Chem. Educ.* **2016**, *93*, 275−286.
(14) Adam, W.; De Lucchi, O.; Hill, K. Reaction of 4-phenyl-1,2,4-triazoline-3,5-dione (PTAD) with Bicyclic Monoterpenes. *Chem. Ber.* **1982**, *115*, 1982−1989.
(15) Suld, G.; Price, C. C. Thiabenzene. I. 1,2,4,6-Tetraphenylthiabenzene. A New Conjugated Ring System. *J. Am. Chem. Soc.* **1961**, *83*, 1770−1771.
(16) (a) Potts, K. T.; Sorm, M. Mesoionic Compounds. XVI. 1,4-Dipolar Type Cycloaddition Reactions Utilizing Pyrimidinium Betaines. *J. Org. Chem.* **1972**, *37*, 1422−1425. (b) Wasserman, H. H.; Pavia, D. L. Reaction of 2,4,6-Triphenylpyrylium 3-Oxide with Oxygen. *J. Chem. Soc. D* **1970**, 1459−1460.
(17) Frisch, M. J.; Trucks, G. W.; Schlegel, H. B.; Scuseria, G. E.; Robb, M. A.; Scalmani, J. G.; Barone, V.; Mennucci, B.; Petersson, G. A.; Caricato, H. M.; Li, X.; Hratchian, H. P.; Izmaylov, A. F.; Zheng, J. G.; Sonnenberg, J. L.; Hada, M.; Ehara, M.; Fukuda, K. R.; Hasegawa, J.; Ishida, M.; Nakajima, T.; Honda, Y.; Nakai, O. H.; Vreven, T.; Montgomery, J. A.; Peralta, J. E.; Bearpark, F. M.; Heyd, J. J.; Brothers, E.; Kudin, K. N.; Staroverov, V. N.; Kobayashi, R.; Normand, J.; Raghavachari, K.; Rendell, A.; Burant, J. C.; Iyengar, S. S.; Tomasi, J.; Cossi, M.; Millam, N. M.; Klene, M.; Knox, J. E.; Cross, J. B.; Bakken, V.; Jaramillo, C. A.; Gomperts, R.; Stratmann, R. E.; Yazyev, O.; Austin, A. J.; Cammi, R.; Pomelli, C.; Ochterski, J. W.; Martin, R. L.; Morokuma, K.; Zakrzewski, V. G.; Voth, G. A.; Salvador, P.; Dannenberg, J. J.; Dapprich, S.; Daniels, A. D.; Farkas, O.; Foresman, J. B.; Ortiz, J. V.; Cioslowski, J.; Fox, D. J. *Gaussian 09*, revision D01; Gaussian Inc.: Wallingford, CT, 2009.
(18) (a) Becke, A. D. A New Mixing of Hartree-Fock and Local Density-functional Theories. *J. Chem. Phys.* **1993**, *98*, 1372−1377. (b) Becke, A. D. Density-Functional Thermochemistry. III. The Role of Exact Exchange. *J. Chem. Phys.* **1993**, *98*, 5648−5652. (c) Lee, C.; Yang, W.; Parr, R. G. Development of the Colle-Salvetti Correlation-energy Formula into a /functional of the Electron Density. *Phys. Rev. B* **1988**, *37*, 785−789. (d) Greer, E. M.; Kwon, K. Overview of Computational Methods for Organic Chemists. In *Applied Theoretical Organic Chemistry*; Tantillo, D. J., Ed.; World Scientific, 2018; pp 31−67.
(19) Dennington, R.; Keith, T.; Millam, J. *GaussView 5*; Semichem Inc: Shawnee Mission KS, 2009.
(20) Fukui, K. The Path of Chemical Reactions—The IRC Approach. *Acc. Chem. Res.* **1981**, *14*, 363−368.

DOI: 10.1021/acs.joc.9b02137
J. Org. Chem. 2019, 84, 14670−14678